The Fluid Dynamics of Reverse Roll Coating

The flow in the metering gap of a reverse roll coater is examined by experiments and finite element solutions of the Navier-Stokes equations. At high speed ratios and capillary numbers, the metered film flow deviates strongly from predictions of lubrication theory: the wetting line moves through the gap center and the metered film thickness passes through a minimum. The two flow instabilities found are ribbing, a sinusoidal cross-web waviness extending smoothly down-web; and cascade, an irregular V-shaped cross-web wave, repeated quasiperiodically down-web. Experimental operability diagrams define parameter ranges where these instabilities and the steady two-dimensional flow are encountered. Ribbing behavior is understood by consideration of the pressure gradient at the free surface. The mechanism of cascade is the intrusion through the gap of the wetting line, which causes the metered film to thicken and eventually reattach to the metering roll in a cyclical manner.

D. J. Coyle
C. W. Macosko
L. E. Scriven
Department of Chemical Engineering
and Materials Science
University of Minnesota
Minneapolis, MN 55455

Introduction

Reverse roll coating is a technique widely used to coat magnetic media, adhesive tape, films, foils, paper, and paperboard (Booth, 1970; Higgins, 1965). Since its invention nearly 60 years ago (Munch, 1932), it has become an important and common coating method due to its versatility, speed and precision. Perhaps the biggest advantage of a reverse roll coater is its ability to produce uniform wet films as thin as 25 μm (1 mil) at speeds of up to 5 m/s (1,000 ft/min). It is also capable of handling liquids of a wide range of viscosity (0.001 to 50 Pa·s).

In addition to the importance of reverse roll coating as an industrial coating technique, the full theoretical description of this process presents an interesting and challenging fluid mechanics problem. Perhaps this complexity is the reason why there has been no adequate theoretical description published. The only models (Ho and Holland, 1978; Greener and Middleman, 1981) are based on lubrication theory without an adequate incorporation of the effects of the free surfaces, surface tension and the dynamic wetting line; it is true, however, that the simple models can predict the flow rate over a limited, but important, range of parameters. Few experimental data have been published. Broughton et al. (1950) concentrated on the final transfer of the metered film onto the substrate. Ho and Holland (1978) and Benkreira et al. (1981) presented useful data over a quite limited range of parameters, while Greener and Middleman (1981) presented data on a simple model system.

Present Address of D. J. Coyle: General Electric Company, Corporate Research and Development, Schenectady, NY 12301.

It is not only the steady-state operation of a reverse roll coater which is of interest. The uniformity of the metered film is crucial in reverse roll coating because it is this film which is transferred to the flexible substrate and becomes the finished product. The goal of any coating operation is steady, two-dimensional flow of liquid so that the coated film is uniform in thickness. Unfortunately, the desired flow states occupy only a small part of the practical region of parameter space. Three-dimensional, periodic, quasiperiodic or apparently chaotic flow states are more commonly found, as reported by Babchin et al. (1981). As this paper shows, the complexity of the flow patterns is connected strongly to events occurring locally within the gap, near or at the dynamic wetting line, and the free surface of the metered film.

This paper presents a detailed theoretical analysis, along with supporting experiments, which together provide a good description of the operation of a reverse roll coater. The results show that achievable flow states and the complexity of the flow patterns are connected strongly to events occurring locally within the gap, near or at the dynamic wetting line, and the free surface of the metered film. The issue of non-Newtonian rheology is addressed in a separate paper (Coyle et al., 1990a).

Model Reverse Roll Coating Systems

Figure 1 depicts a typical reverse roll coater. Though there are numerous variants, they all operate in basically the same manner. A liquid film is applied to the rigid steel applicator roll either by dipping into a liquid bath (as drawn here), by extruding liquid from some type of die or by transferring liquid from a

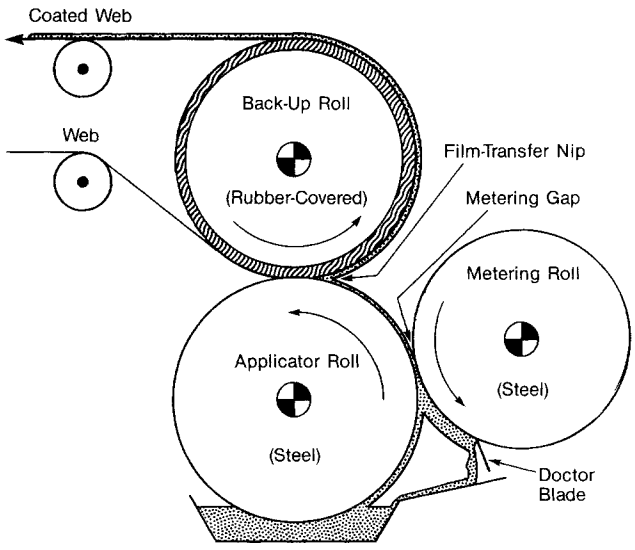

Figure 1. Typical reverse roll coater.
The metering gap is the dominant factor controlling the thickness and uniformity of the coating.

pick-up roll. This film is relatively thick. It is partially wiped off by a rigid steel metering roll whose surface moves in the opposite direction at a distance from the applicator roll surface of about 25 to 250 μm in a region called the metering gap. The liquid within that gap is often called the coating bead. The thin metered film remaining on the applicator roll is subsequently transferred to the web (the substrate to be coated), which is squeezed between the applicator roll and a resilient rubber back-up roll. The initial film application and the final film transfer to the web can both be important processes, but it is the creation of the metered film by the complex flow in the metering gap which is the crux of all reverse roll coating operations. This coating bead flow not only determines the final coating weight, but also is the prime influence on the uniformity of the coated film. Both factors are influenced strongly by the gap, by the applicator roll speed (which is usually not much different from the web speed and thus the production speed), and by the speed ratio between the metering and applicator rolls.

Because the gap between the rolls is much smaller than the diameter of either, the menisci on each side of the gap can be expected to be separated by a region of lubrication-type flow, i.e., of nearly straight streamlines. This suggests decomposing the metering gap into two parts, each of them modeled by a flow between a pair of half-submerged rolls, as depicted in Figure 2. One is the upstream film transfer side of the gap, and the other, the downstream metered film/wetting line side. Each is half-submerged in what can be regarded as an infinite bath of liquid. Hence, a lubrication-flow boundary condition at the gap center (place of least clearance) can be used in the "one-sided" finite element analyses (i.e., those described by Coyle et al., 1986). The third model flow (Figure 2c) contains the entire metering gap and thus can be used to test the half-submerged models. The upstream film-transfer model (Figure 2a) was first examined by Greener and Middleman (1981). It has been shown (Coyle 1984) not to mimick the interesting phenomena of an actual reverse roll coater because this model system has no dynamic wetting line, and so is not considered further here. The half-submerged model flow in Figure 2b can be turned into a complete metering gap flow by lowering the liquid in the bath so that an air/liquid interface forms on the bottom side of the gap.

Experiments were conducted on a specially designed roll coating machine, which consisted of two horizontally mounted, equal-diameter, polished, hard chrome-plated steel rolls driven via timing belts by fractional horsepower DC motors with feedback control. The runout of the rolls (TIR) was less than 2.5 μm (0.0001 in.), and the surface roughness (RMS) was approximately 0.2 μm (8 μin.). The rolls were 0.2 m (8 in.) in diameter by 0.3 m (12 in.) in length and were driven at 0-5 m/s (0-1000 ft/min) surface speeds. The gap between roll surfaces was typically set at 125-1,000 μm (5-40 mil). A micrometer-driven needle was used to measure coating thickness directly. The pilot plant at James River Graphics, Inc., South Hadley, Massachusetts, was used to create the complete metering gap flow depicted in Figure 2c, where the rolls are 0.4 m face by 0.3 m diameter (16 in. face by 12.in. dia.). The main goal there was to take advantage of the superior precision and control in the pilot-plant equipment, which allows for smaller gap settings (clearance between roll surfaces, typically 25 μm or 0.001 in.) and better doctoring of the metering roll. Coating thickness was here measured by collecting the coating after scraping it from

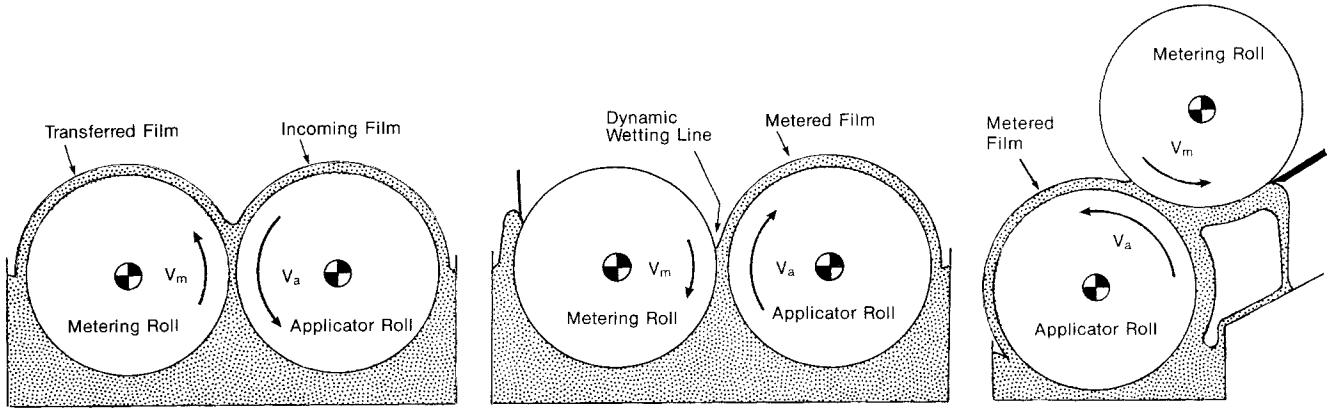

a. Half-submerged film transfer flow

b. Half-submerged metered film flow

c. Pilot coater complete metering gap flow

Figure 2. Model reverse roll coating systems.

the applicator roll. Coating liquids used were glycerine/water and corn syrup/water solutions, with viscosities ranging from 0.1 to 2 Pa·s (100 to 2,000 cp). Further details of the apparatus and methods are given elsewhere (Coyle, 1984).

Analysis of Flow in the Metering Gap

The analysis of the complete metering gap in a reverse roll coater by solution of the Navier-Stokes equations avoids the limitations of lubrication theory and the half-submerged roll models. Neither does it require excluding the wetting line and metered film nor assumes that they are uncoupled from the film transfer flow. One simplification made for the sake of convenience is that gravity is not important, which is valid in the cases of interest. Thus, in the remainder of this work it is irrelevant whether the gap is oriented horizontally or vertically.

The analysis is not without difficulties, the major one being the representation of the film transfer free surface. The higher the capillary number and the thinner the arriving film, the further toward the nip the transfer meniscus recedes, the sharper its curvature, and the more difficult its parameterization by spines and representation by finite element basis functions. A typical finite element discretization of the Navier-Stokes system for this flow had 120 elements and 1,300 unknowns. A representative discretization is shown in Figure 3a: in this instance, the thickness of the arriving film was set (somewhat arbitrarily) at 1.25 gap widths.

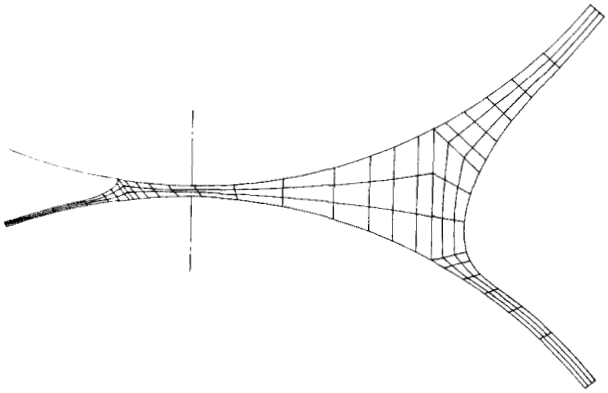

Figure 3a. Finite element discretizations.

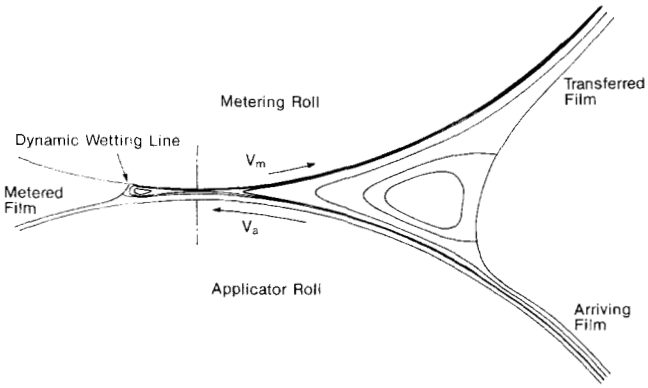

Figure 3b. Predicted streamlines: flow in the metering gap including both free surfaces showing two closed recirculations (Ca = 0.1, R/H_o = 100, V_m/V_a = 0.5).

As the streamlines at low speed ratio (Figure 3b) illustrate, there can indeed be a parallel-flow region that separates the flow fields near the free surface at each side of the gap. There is a large recirculation on the upstream film transfer side of the gap, and a smaller one may appear in the diverging flow region near the dynamic wetting line. The streamline plot also shows that the metered film develops rapidly into its final plug-flow regime.

The speed ratio is one of the most important parameters of this flow. Figure 4 shows that increasing the speed ratio pulls the wetting line through the gap, causes the recirculations to shrink, and changes the large coating bead into one that is small, tightly-curved, and located entirely to one side of the gap. It is exactly this qualitative behavior that is confirmed by the photographs in Figure 5. The capillary number is the second important parameter. Increasing its value has much the same effect as increasing the speed ratio, as shown in Figure 6. One subtle difference is that increasing the capillary number causes the recirculations to virtually disappear, whereas at high speed ratio they persist at significant intensity though they are smaller in size.

The flow rate through the gap or the metered film thickness is the primary dependent variable of interest. It is convenient to define the dimensionless metered film thickness (t) as the metered film thickness divided by the total gap width. When the free surfaces are ignored and lubrication theory is applied, it is a simple matter to derive a relationship for the metered film thickness (Ho and Holland, 1978):

$$t = \frac{2}{3}\left[1 - \frac{V_m}{V_a}\right] \qquad (1).$$

As established by the results of computations and experiments shown in Figure 7a, the film thickness at low speed ratio lies close to the lubrication model, but as speed ratio increases, the film thickness goes through a minimum and begins to *increase*

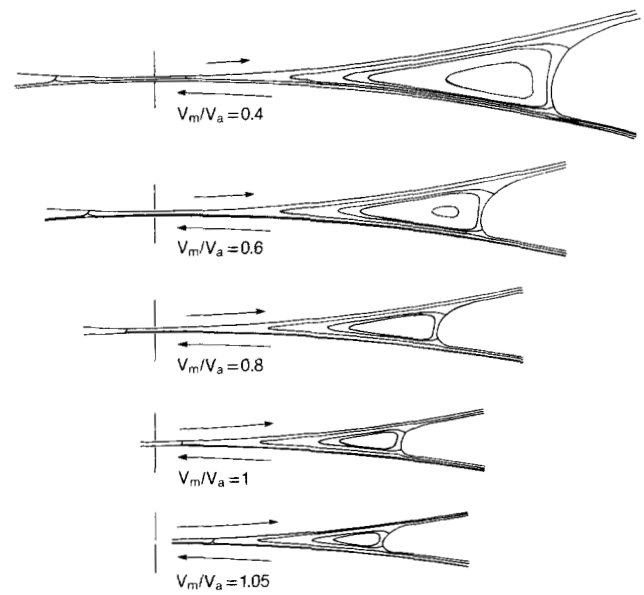

Figure 4. Effect of speed ratio on metering gap flow streamlines (Ca = 0.1, R/H_o = 1,000).

Increasing speed ratio "pulls" the dynamic wetting line completely through the gap, shrinking the size of the bead, though the recirculation persists.

a. $V_m/V_a = 0.74$

b. $V_m/V_a = 1.67$

c. $V_m/V_a = 2.83$

Figure 5. Reverse roll coating bead at speed ratios.

They show the same qualitative behavior of the bead as predicted in Figure 4.
Courtesy of Willem Nikkel, Westvaco Covington Research Laboratory, Covington, VA.

with increasing speed ratio. At higher capillary number, the minimum appears at lower speed ratio and is sharper, as shown by the experimental results displayed in Figure 7b. The data of Ho and Holland (1978) are restricted to low speed ratios ($0.07 < V_m/V_a < 0.37$) and also agree closely with lubrication theory (Eq. 1); however, those authors made no mention of what happens at higher speed ratios. Similarly, the data of Benkreira et al. (1981) also agree with Eq. 1 (with a coefficient of 0.63), but these investigators too must have restricted their measurements to low speed ratio.

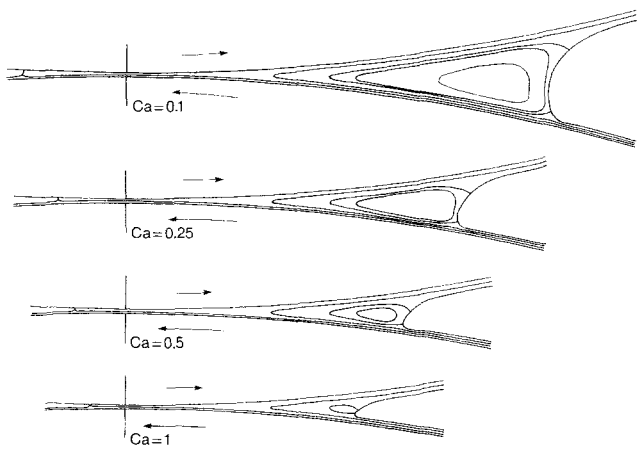

Figure 6. Effect of capillary number on metering gap flow streamlines (R/H_o = 1,000, V_m/V_a = 0.4).

Increasing the capillary number shrinks the bead and eliminates the recirculations.

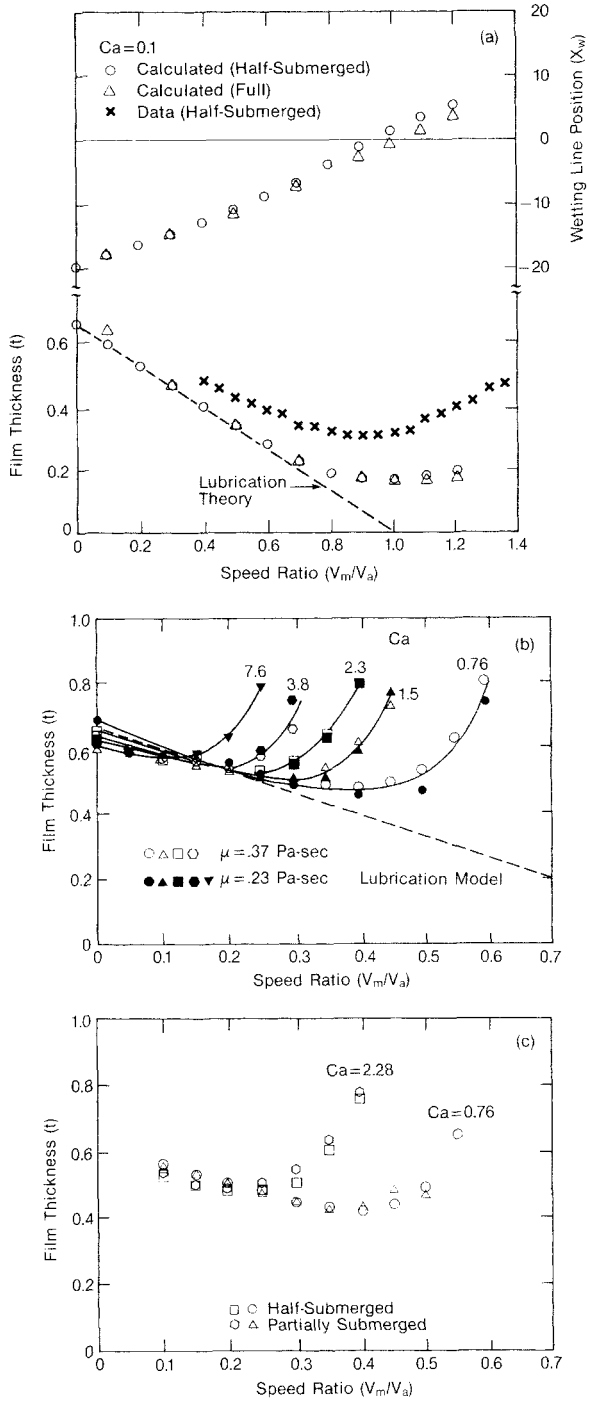

Figure 7. Metered film thickness as a function of speed ratio and capillary number.

Calculations (a) and experiments (c) show no significant difference between the complete metering gap flow and the half-submerged system. Experiments (a, b) show the flow rate minimum and its dependence on capillary number.

At first glance, these results are perplexing. Capillary number is defined as $Ca = \mu V_a/\sigma$; so, high Ca corresponds to low surface tension and, presumably, negligible effects of free surfaces. This might lead to the conclusion that the higher the capillary number, the more accurate the lubrication approximation. Yet, this is the opposite of the Navier-Stokes predictions. The reason for this capillary number dependence is as follows. The pressure

jump across a meniscus is the curvature times the surface tension, and thus is inversely proportional to the capillary number. Higher capillary number corresponds to a more strongly curved surface at the same pressure jump. Hence, the free surface of the metered film can move into, and even through, the center of the gap between the rolls. When the dynamic wetting line passes through the gap center and locates on the upstream (feed) side of the gap, the gap itself is partially filled with air. This configuration greatly decreases the lubrication effect of the two nonparallel moving solid surfaces, and the lubrication model fails. In short, the weaker the surface tension—the higher the capillary number—the more important the free surfaces become because they move and, in doing so, change the domain of the flow.

If the flow in a reverse roll coater is controlled by the flow near the metered film and the wetting line, the half-submerged model of Figure 2b should be an accurate model of the actual metering gap flow. To solve the Navier-Stokes equations for this flow, the finite element discretization shown in Figure 3a was truncated at a fixed distance from the wetting line. At this upstream end of the finite element domain, a lubrication boundary condition was imposed on the velocity and pressure fields (cf. Coyle et al., 1986). Computed predictions revealed that the pressure profile becomes one-dimensional within 1 to 3 gap widths upstream of the wetting line. Consequently, the distance from the wetting line to the place where the lubrication boundary condition was imposed was chosen to be 5 gap widths. The 500 unknowns used in this calculation are considerably fewer than proved necessary to treat the entire metering gap. At the same time, the predictions of the flow rate and wetting line position are virtually the same as in the complete analysis, as shown in Figure 7a. The experimental results displayed in Figure 7c confirm that the half-submerged system results in identical film thicknesses. Thus, it is the flow in the region of the wetting line and the formation of the metered film which is of primary importance in a reverse roll coater. The relevance of these effects to the stability of the flow is developed later.

An unusual, but practically important, operating condition for a reverse roll coater is a low viscosity liquid, speed ratio greater than unity, and an arriving film on the applicator roll which is thinner than the minimum gap clearance. This case

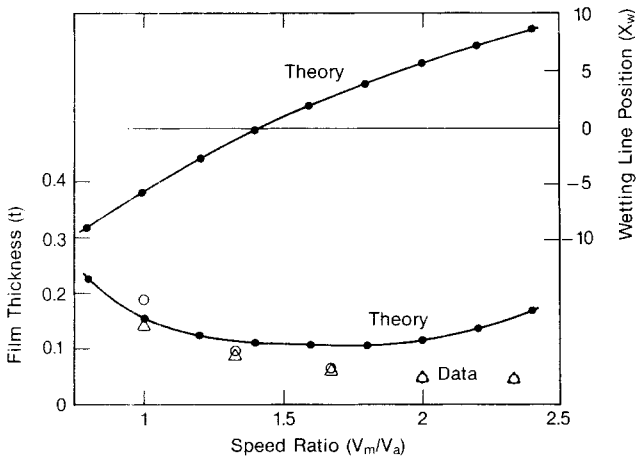

Figure 8. Operation of a reverse roll coater at high speed ratio and low capillary number.

$Ca = 0.005$, $R/H_o = 1{,}000$, duplicate runs. Data courtesy of Diana Zimny, 3M Co., St. Paul, MN.

demonstrates how very thin coatings can be achieved ($t < 0.05$) and also shows where the upstream film transfer flow is *not* negligible. The data in Figure 8 indicate that stable operation is possible at speed ratios of 1 to 2 when the capillary number is on the order of 0.005 or less. The theoretical calculations for the corresponding parameter values predict the observed thin films. The wetting line passes through the gap center at a speed ratio of about 1.4. As speed ratio is increased further, the coating bead ultimately breaks since the inlet film is thinner than the gap for these experiments. The data at these parameter values also show that the inlet film thickness can sometimes strongly affect the metered film thickness, namely for the unusual conditions when the inlet film is thinner than the gap. As shown in Figure 9, the metered film gets thinner as the inlet film thickness is decreased below 1 gap width.

There is an important point to be noted about the Navier-Stokes system as employed here. The physics at the dynamic wetting line is not fully understood, although there is evidence that entrainment and breakdown of a submicroscopic air film gives rise to apparent slip and an effective dynamic contact angle (Miyamoto and Scriven, 1982; Miyamoto, 1986; Mues et al., 1989). Be that as it may, to complete the Navier-Stokes system, two conditions must ordinarily be imposed at the dynamic wetting line. First, for finite capillary number, the apparent dynamic contact angle (θ_c) must be specified (see, for example, Kistler and Scriven, 1983). Second, the aphysical stress singularity, which the no-slip boundary condition produces at the wetting line, must be relieved. This can be done by allowing some slip near the wetting line, as discussed by Huh and Scriven (1971), Dussan and Davis (1974), Dussan (1976), and Hocking (1976, 1977). A physically plausible choice is Navier's (1827) boundary condition which states that the normal flux of the momentum component tangential to the solid surface is proportional to the velocity discontinuity there. The proportionality constant B is a slip coefficient and is the reciprocal of a momentum transfer coefficient. The constant value of $B = 0.01$ was chosen for all calculations. This allows a fair comparison of

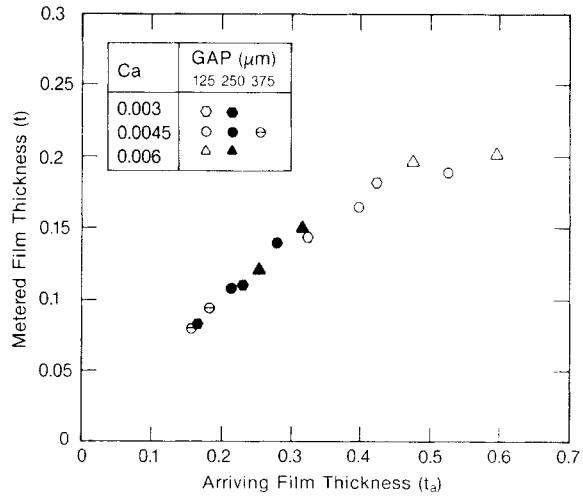

Figure 9. Dependence of measured metered film thickness on the arriving film thickness, showing that if the latter is much thinner than the gap then the metered film is strongly affected.

$R/H_o = 1{,}000$, $V_m/V_a = 1.0$. Data courtesy of Diana Zimny, 3M Co., St. Paul, MN.

predictions at various values of the other parameters, because the important trends can be examined without the interference of varying slip. The characteristic slip length corresponding to $B = 0.01$ under conditions of interest here is on the order of 1 μm. Kistler (1983) and Kistler and Scriven (1983) discuss in greater detail the case for slip at dynamic wetting lines, the relevant literature, and the implications to finite element calculations of viscous free-surface flows.

The uncertainties about conditions at the dynamic wetting line make somewhat uncertain the reliability of quantitative predictions of the flow field in reverse roll coating. Nevertheless, the comparisons with experimental data make it plain that the predicted flow field and trends with parameter variations are represented accurately. For example, the important fact that the flow rate goes through a minimum as speed ratio increases is predicted regardless of the slip coefficient and contact angle chosen. Only the *exact* value of speed ratio at which this minimum occurs cannot be predicted *a priori*. The same is true of other important features of these flows.

From solutions of the full Navier-Stokes equations the viscous traction and pressure at the roll surfaces can be calculated, and thus important forces and torques can be predicted. For example, owing to the converging flow geometry, roll coaters can develop high pressures that produce large forces tending to push the rolls apart. These forces can be large enough to bow steel rolls in the center, causing the film thickness to vary across the width of the substrate.

Lubrication theory suggests a convenient definition of dimensionless force

$$f = \frac{\int p\, dx}{\mu V_a}\left(\frac{H_o}{R}\right) \tag{2}$$

Lubrication theory cannot be used to evaluate this force for two reasons:

1. It does not always accurately predict the flow rate, which strongly affects the pressure profiles to be integrated.

2. The wetting line position and thus one of the limits of integration in Eq. 2 remains unknown when lubrication theory is resorted to.

Computations show that the dimensionless force, as defined by Eq. 2, is virtually constant for roll diameter/gap ratios greater than 1,000 and therefore is independent of the gap for most, if not all, practical applications. The force also is constant over capillary numbers greater than unity, but falls significantly as capillary number drops below unity.

The roll-separating force decreases with increasing speed ratio, as shown in Figure 10. At low enough capillary numbers, the roll-separating force turns negative: in other words, the rolls are drawn together. This unusual behavior has actually been observed in a reverse roll flow where the applicator roll was replaced by a suspended, deflectable web (Rose, 1975).

So far, only the two-dimensional steady-state behavior of a reverse roll coater has been discussed. In reality, such flows occur only in certain regions of parameter space. For other parameter values, the observed flows are three-dimensional and sometimes time-dependent, resulting in nonuniform coatings. The rest of this paper deals with these flow instabilities—both their sensitivity to parameters and their underlying mechanisms.

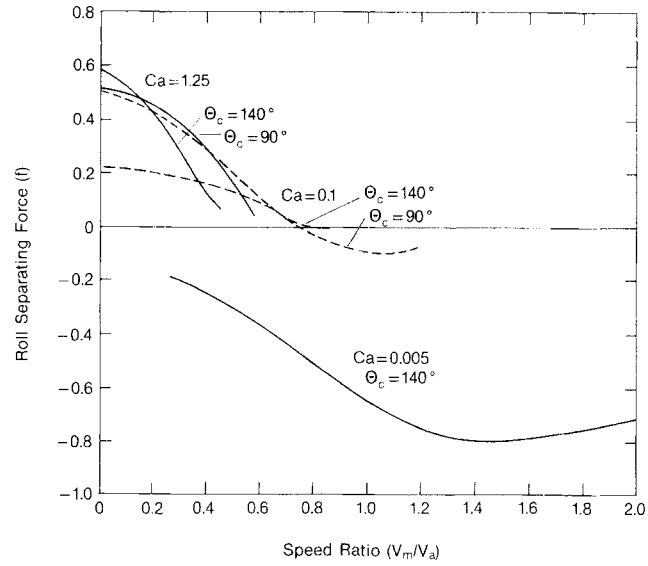

Figure 10. Predicted roll separating force as a function of speed ratio, capillary number, and specified contact angle (R/H_o = 1,000).

Flow Instabilities in Reverse Roll Coating

The photographs of the metered film in Figure 11 are of the two most common flow states, along with the elusive uniform film flow. The liquid is Newtonian, the applicator roll speed is fixed, and the metering roll speed is being increased from (a) to (c). At low ratios of metering roll speed to applicator roll speed the film is noticeably ribbed (a): that is, it carries the same down-web, uniformly-spaced, "rake-lines" or "corduroy" or "phonographing" that is seen in forward roll coating (cf. Pitts and Greiller, 1961). As the speed ratio is raised, the amplitude of the ribs decreases and in some cases the film becomes uniform to the naked eye (b). At still higher ratios, an instability called "cascade," "herringbone," or "seashore" sets in (c). This is a periodic cross-web disturbance, but each cross-web bar is uneven in the transverse direction. When the gap between the rolls is smaller, the bars are closer together. The striking wave pattern in (c) shows the sharp contrast between regions of thin and thick film. Booth (1970) reported that "concentric rings" appeared if the metering roll is too slow and a "rough wavelike pattern," if the metering roll is too fast; Babchin et al. (1981) report the same type of behavior when non-Newtonian starch-based adhesives are used. In other published studies of reverse roll coating (Benkreira et al., 1981; Ho and Holland, 1978), no flow instabilities were mentioned.

An important observation in the present study is that, when the cascade pattern is observed on the metered film, large air bubbles are entrained at the wetting line on the metering roll. The bubbles are several times larger than the roll gap, suggesting a mechanism different from that responsible for entrainment of strings of tiny air bubbles in plunging tape experiments (Burley and Kennedy, 1976; Blake and Ruschak, 1979) or curtain coating (Kistler, 1983). In addition, if the rolls are not half-submerged, the entire coating bead can be seen to oscillate at the same frequency as the cross-web bars on the metered film. These observations prove to be a key in understanding the mechanism of cascade.

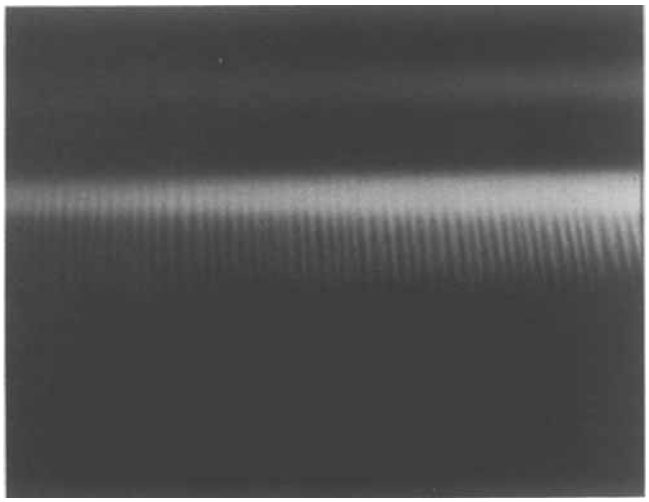

a. Ribbing (front view), gap = 1 mil, Ca = 0.52, $V_m/V_a = 0.1$

b. Uniform film (side view), gap = 1 mil, Ca = 0.31, $V_m/V_a = 0.38$

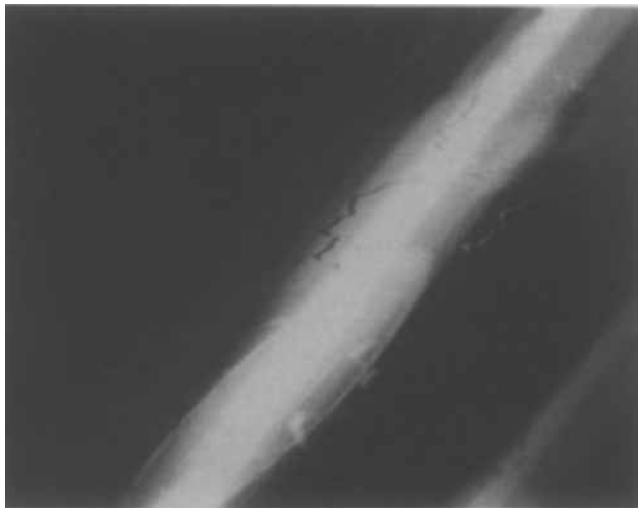

c. Cascade (top view), gap = 2 mil, Ca = 0.21, $V_m/V_a = 0.56$

Figure 11. Metered film on the pilot reverse roll coater

Liquid is Newtonian corn syrup/water mixture, $\mu = 0.33$ Pa·s.

Stability Diagrams for Reverse Roll Coating

A stability diagram graphically shows regions in parameter space where various flow states are found. In certain regions, a two-dimensional steady-state uniform film flow may be stable and thus be the flow state experimentally observed. In other regions, this flow state is unstable, such as in the regions where ribs or cascade are found. Since the uniform flow region represents the desired operating conditions for a coating device, these diagrams are often called operability diagrams. The boundaries between the stable region and the various "instabilities" define the operability limits of the coater.

The two most important parameters in reverse roll coating are the ratio of roll surface speeds and the ratio of viscous to surface tension forces. Therefore, the two most important dimensionless groups are the speed ratio (V_m/V_a) and the capillary number ($Ca = \mu V_a/\sigma$). Figure 12 is a representative stability diagram for a reverse roll coater. The case of $V_m/V_a = 0$ (the Y-axis) is one roll turning alongside a stationary one and is similar to a wedge spreader moving over a flat surface (see Pearson, 1960). At very low capillary numbers, the film is uniform, but it is ribbed at capillary numbers greater than that of point A. If the speed ratio is increased, the ribs disappear as the curve BC is crossed. If the speed ratio is further increased, the uniform film flow is replaced by the cascade instability as curve DE is crossed. The photographic sequence in Figure 11 corresponds to increasing speed ratio at a capillary number greater than A in Figure 12. The range of speed ratios over which uniform films are found is the "speed window" referred to by Babchin et al. (1981).

Another interesting feature is the stability behavior at low capillary number. Consider, for example, operation at a constant speed ratio. If the capillary number is small (point 1), the flow is stabilized to ribbing by decreasing the production rate (which is proportional to V_a and thus Ca). But as somewhat higher Ca (point 2), the flow is stabilized to ribbing by *increasing* the production rate. Next, consider operation at a constant capillary number. If the speed ratio is large (point 4), the flow is stabilized to ribbing by increasing the speed ratio. But at lower speed ratio (point 3), the flow is stabilized to ribbing by *decreasing* the speed ratio. In both examples, the latter choice is counterintuitive, and there can be other options as well. Moreover, the curves in Figure 12 shift considerably as other parameters change (such as the gap and the Reynolds number) so that the stable region can be enlarged, shifted in location, or even eliminated for all but the lowest capillary numbers. Thus, it is important to examine the stability diagram and its dependence on parameters in order to understand the operability of a reverse roll coater.

Figure 13 shows the effect of gap width on the stability of the flow of Newtonian glycerine/water solutions in the half-submerged configuration of Figure 2b. The onset of cascade is relatively insensitive to the gap, whereas the dividing line between ribbed and uniform films is quite sensitive. As the gap is reduced, the stable region greatly shrinks, with the low capillary number stable region disappearing below the lower limit of the data. There are ranges of capillary number in which no stable flow is possible; as the speed ratio is increased, cascade appears before the ribs have disappeared. Figure 13 also shows that data with liquids of viscosities of 0.2 to 0.4 Pa·s viscosities overlap, indicating that here the capillary number is the only dimensionless group of significance into which the viscosity enters.

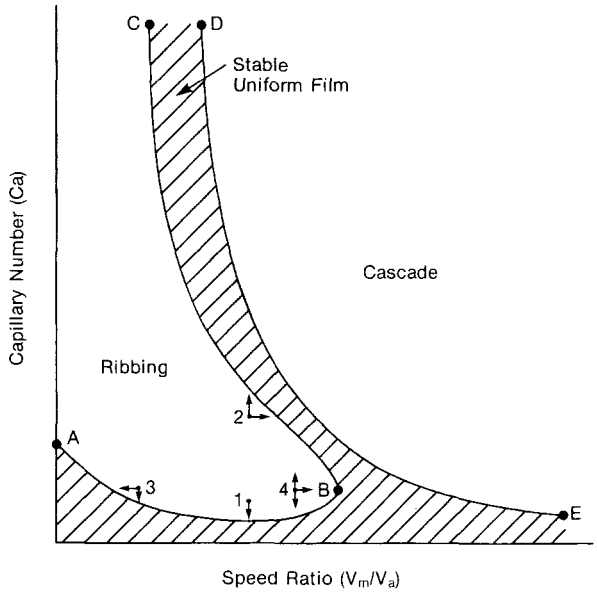

Figure 12. Typical stability diagram for the metered film in reverse roll coating.

To evaluate the effect of the film transfer free surface flow on the stability of the metered film flow, the liquid level in the bath was lowered so that the rolls were submerged only 3 cm. The inlet film on the film transfer side was on the order of 750 μm (30 mil) in the experiments summarized in Figure 14. The overlap of the measurements with those from the half-submerged experiments indicates that the presence of the upstream film transfer meniscus has little effect on the stability of the metered film, at least as long as the gap is narrower than the thickness of the inlet film. Because typical reverse roll coater gaps are on the order of 1 mil, inlet film thicknesses are typically much greater than the gap, and thus the half-submerged metered film flow is an accurate model of the full flow.

The onset of cascade was also measured on the pilot coater of Figure 2c. The Newtonian fluids used were mixtures of corn syrup and water. The results are summarized in Figure 15. At a given capillary number, the speed ratio at the onset of cascade decreases only slightly as the gap is increased. The solid line is a fit of the data from the pilot coater

$$Ca = \frac{0.16}{(V_m/V_a)^{2.16}}, \quad 0.2 < Ca < 4 \tag{3}$$

Only the data at high capillary numbers obtained with the University of Minnesota laboratory roll coater deviate from this line (Figure 15b). The metering roll was doctored by a flexible polyurethane squeegee which left behind a thin liquid film at high speeds (approximately 5 μm thick, as measured by absorbing a known area of the film with a tissue and weighing the fluid collected). The presence of this film must alter the wetting line and so shift the onset of cascade to higher speed ratios. When, at the

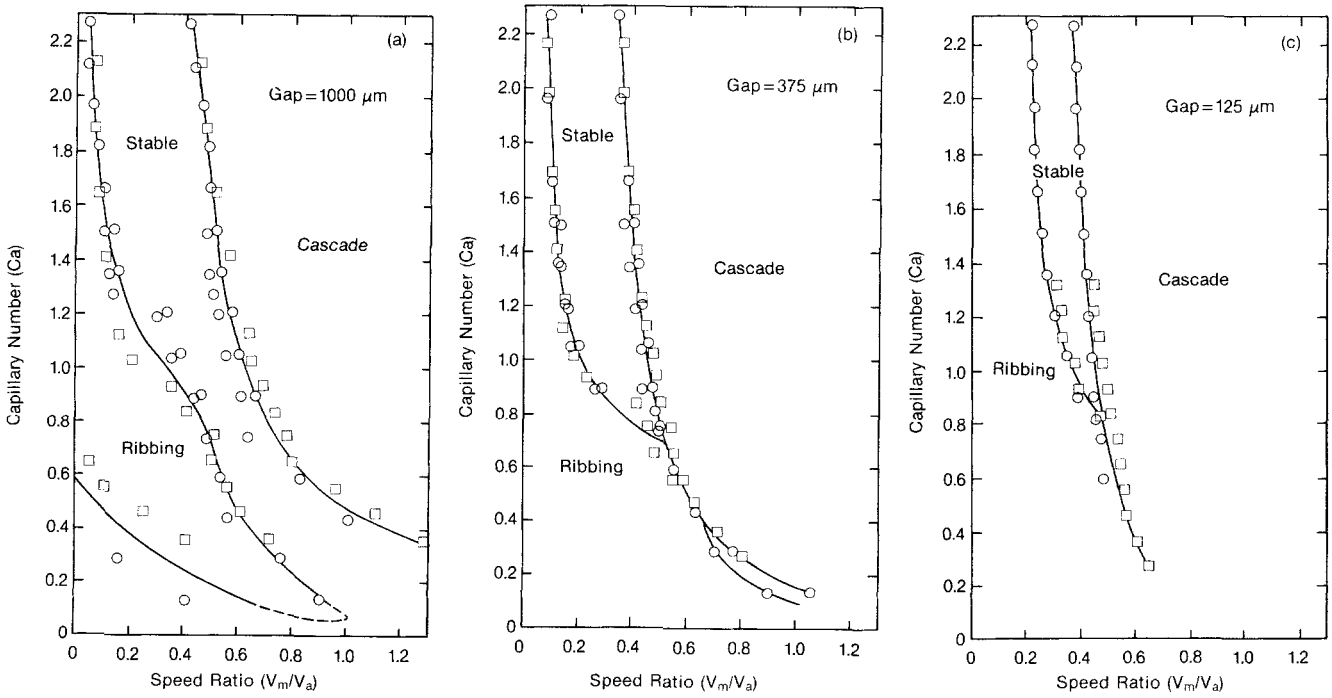

Figure 13. Experimental stability diagrams of half-submerged metered film flow as a function of the gap.
O—μ = 0.4 Pa·s, □—μ = 0.2 Pa·s

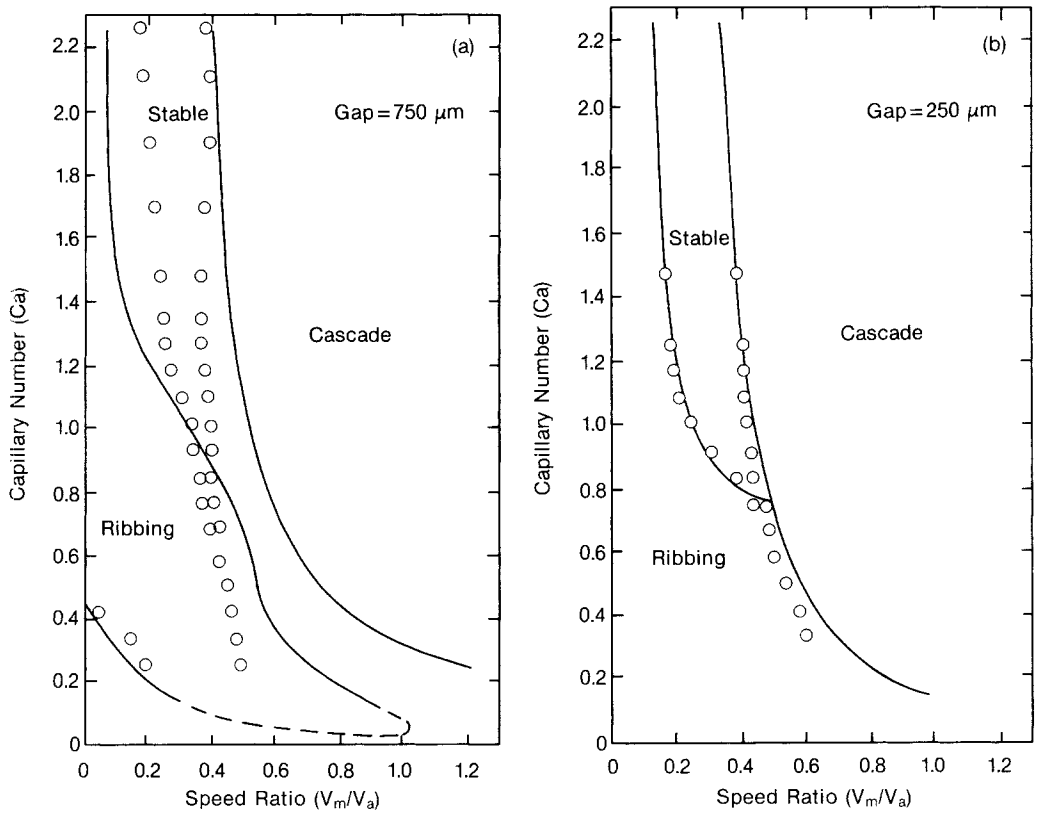

Figure 14. Comparison of stability diagrams for partially-submerged (○) and half-submerged (—) metered film flows as a function of the gap.

onset of cascade, this film was manually removed by rapid wiping of the metering roll surface with an absorbent tissue, the cascade pattern disappeared. The scraper on the pilot coater was made of rigid ultra-high-molecular-weight polyethylene and was pressed to the roll (at a plowing angle as shown in Figure 1) with approximately 45 kg (100 lb) force over its 432 mm (17 in.) length; this is enough loading to scrape the metering roll virtually dry.

It should be noted that no stable, uniform flow region was observed on the pilot coater. Instead, ribs visible to the naked eye were always present when cascade was not, although these ribs were very small in amplitude and difficult to see (Figure 11b) at parameter values for which uniform films were observed in half-submerged flow.

Nature of the Ribbing Instability

A simple argument can be used to deduce the stability of a free surface flow to ribbing (see Pearson, 1960; Pitts and Greiller, 1961; Savage, 1977). By considering the balance between surface tension forces (capillary pressure) and viscous forces (reflected by the pressure gradient in the streamwise direction), a criterion can be developed for stability, namely

$$\frac{dP}{ds} < \frac{1}{Ca}\left[\frac{1}{r^2}\frac{dr}{ds} + N^2\right] \tag{4}$$

where

r = radius of curvature of the meniscus
N = dimensionless wavenumber of the (rib) disturbance
s = streamwise cooridate in the direction from the gap to the free surface

The right side of Eq. 4 is positive so that surface tension stabilizes the flow with respect to ribbing. The stability of the flow to ribbing can now be deduced by considering the pressure gradient term alone. Finite element analyses can be used to describe the two-dimensional metered film flow, and thus one can estimate whether or not the flow is stable by examining the predicted pressure gradient at the meniscus.

Equation 4 implies that the more steeply the pressure increases in the flow direction s (towards the meniscus), the greater the tendency of the flow to be ribbed. In other words, the two-dimensional flow is more unstable. On the other hand, if the pressure decreases in the flow direction, the flow is stable to ribbing. The pressure profiles in Figure 16 reveal that the flow should be unstable to ribbing at a low speed ratio that depends on the magnitude of the surface tension term, but should turn stable to ribbing as the speed ratio is increased. This was observed at high capillary number (Figures 13 and 14), except that the cascade instability may have set in before the speed ratio was high enough to make the flow stable to ribbing. Figure 17 shows the pressure gradient at the meniscus as a function of speed ratio and capillary number. At high Ca, the flow becomes stabilized as speed ratio is increased. At low Ca, the flow first becomes destabilized as speed ratio is increased, before finally becoming stabilized again at high enough speed ratio. Thus, the evolution of the pressure gradient provides a physical explanation of the "peninsula" of ribbed flow regimes in Figures 12–14.

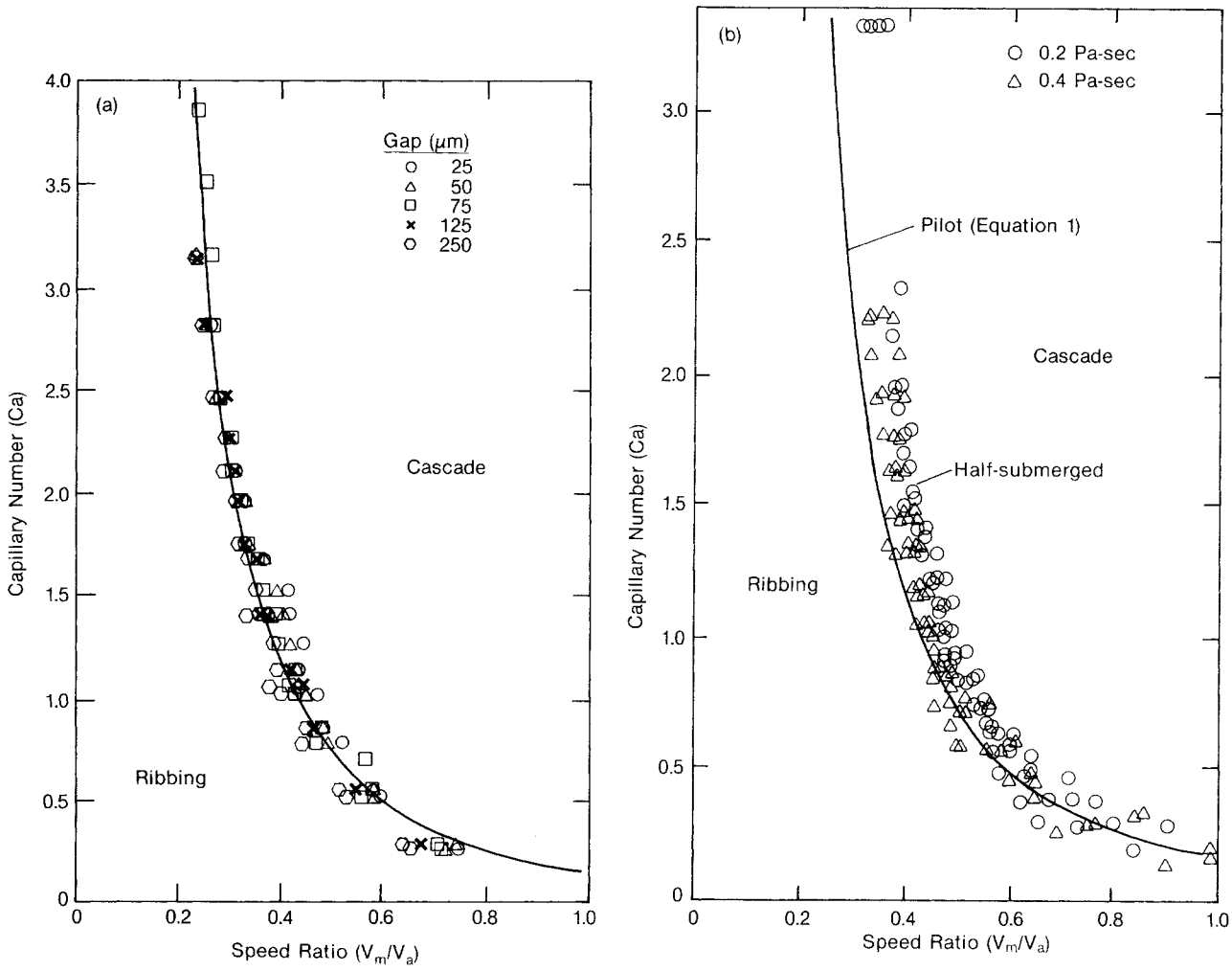

Figure 15. Experimental onset of cascade at various gap settings in pilot metering gap flow (a), and (b) comparison with half-submerged data.

The solid line is from Eq. 3.

As mentioned earlier, a uniform film was not observed on the pilot coater. Instead, at parameter values corresponding to the uniform film flow in the half-submerged experiments, very small amplitude ribs could be observed (with difficulty). A possible explanation for these slightly differing results is that near the apparent onset of ribbing, gravity can be a significant stabilizing force (Coyle et al., 1990b). In the half-submerged configuration, gravity acts straight down from the meniscus toward the gap and thus is most effective at creating a stabilizing pressure gradient. In the pilot configuration, gravity acts nearly perpendicular to the gap and therefore has much less stabilizing influence. In all experiments, as speed ratio changed there was no abrupt onset of ribbing, just a gradual change in rib amplitude, which made the distinction between ribbed and uniform films difficult. A further complication was that the meniscus could not be viewed well near the wetting line, where disturbances were largest; instead, observations had to be made much further downstream where they may have had time to level.

Thus, small inaccuracies in visual detection and the influence of gravity may have large effects on the measured onset of ribbing. In a practical coating operation, it is probably much more useful to think of the film as always ribbed (if cascade is not present). The regions labeled "stable" exhibit much smaller amplitude disturbances which may level to an acceptable degree before the final product solidifies from drying, chilling, or curing.

The preceding heuristic stability argument works well for Newtonian liquids, but when applied to shear-thinning and elastic liquids it may not hold true. This point is considered in a separate paper (Coyle et al., 1990a). The next section examines the second major instability in reverse roll coating—the cascade instability.

Mechanism of the Cascade Instability

The cascade instability is a large-amplitude, three-dimensional, time-periodic disturbance of the metered film. Whereas small-amplitude ribbing can be acceptable from a practical point of view, if it is slight enough or levels rapidly enough, cascade is unacceptable in applications. This instability is closely associated with the events near or at the dynamic wetting line deep within the gap, and thus was not directly observable in the experiments. The pattern of the metered film (Figure 11c) suggests some sort of cyclic phenomenon during which air is

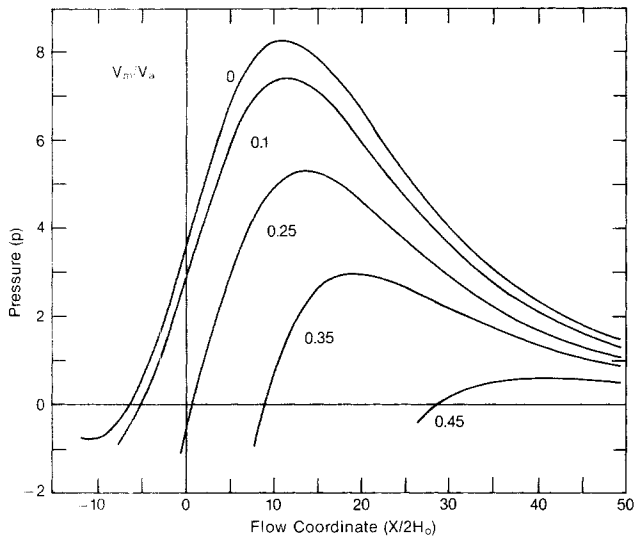

Figure 16. Pressure profiles as a function of speed ratio as predicted by finite element solution of the Navier-Stokes equations.

The streamwise coordinate s runs from right to left: $Ca = 1.25$, $Re = 0$, $St = 0$, $R/H_o = 1{,}000$, $\theta_c = 140°$.

entrained. In order to understand the mechanism of the cascade instability certain aspects of the steady metered film flow must be examined further.

The computed flow fields presented earlier do not extend into the region of cascade. The Navier-Stokes predictions of the metered film thickness or flow rate at high speed ratios display some remarkable features. Figure 18 shows the minimum in the film thickness as before, but as speed ratio is increased further the film thickness rises abruptly.

Though the exact location of this steeply changing portion of the curve depends on the value of dynamic contact angle which is chosen, the calculated film thickness at high speed ratio

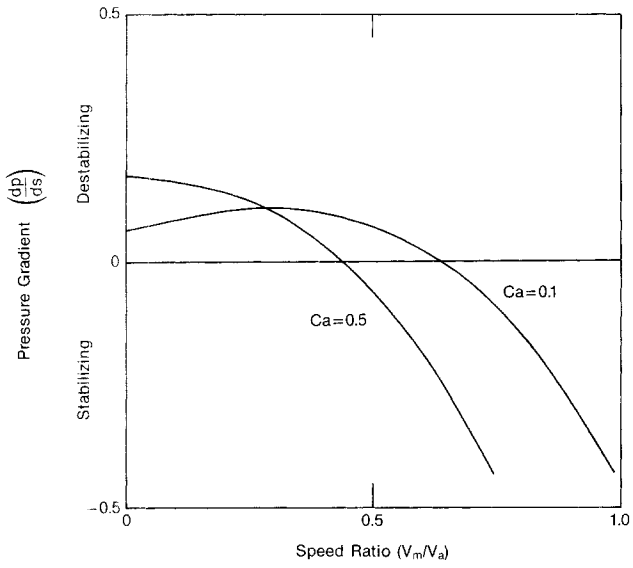

Figure 17. Computed pressure gradient at metered film meniscus as a function of speed ratio and capillary number.

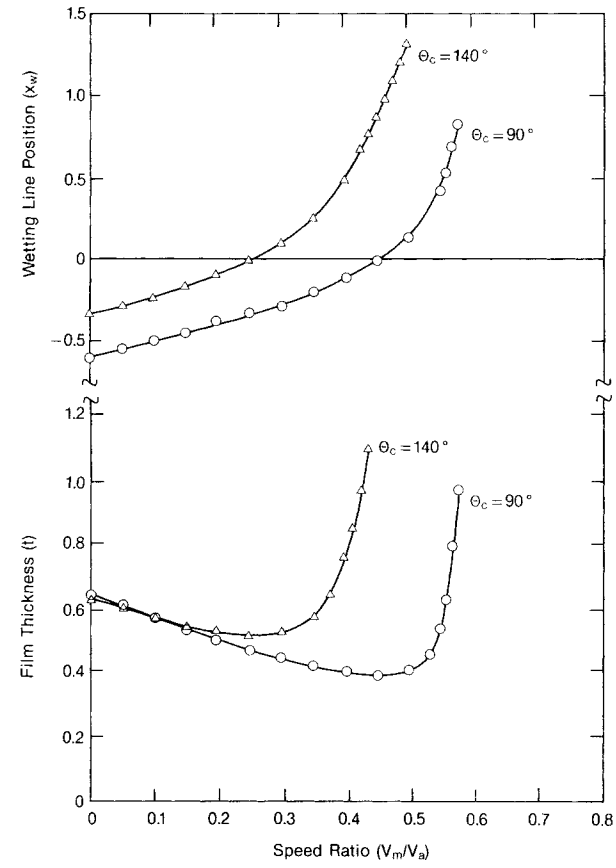

Figure 18. Metered film thickness and wetting line position as predicted by finite element solution of the Navier-Stokes equations ($Ca = 1.25$, $Re = 0$, $St = 0$, $R/H_o = 1{,}000$).

always becomes much thicker than the gap between the rolls. Figure 18 also shows that the position of the wetting line moves through the gap as speed ratio is increased. This behavior can be used to explain the shape of the flow rate curve as follows.

According to models based on lubrication theory, the metered film thickness should decrease linearly with increase speed ratio (Eq. 1). This is accurate at low speed ratio as long as the wetting line position is on the metered film side of the gap ($x_w < 0$), and thus the region of minimum roll separation is filled with liquid. But as the speed ratio increases, the wetting line position moves to the film transfer side of the gap ($x_w > 0$); the minimum roll surface clearance seen by the liquid is at the wetting line. This larger minimum clearance directly results in a thicker metered film. In addition, at higher speed ratios the wetting line position is more sensitive to speed ratio; thus, the upturn in film thickness is steep.

Figure 19 shows computed free surface profiles at three values of speed ratio. These theoretical predictions indicate that the onset of the cascade instability proceeds as follows. Comparing (a) and (b) shows how at low speed ratio the film thins as speed ratio increases, while at the same time the wetting line moves closer to the center of the gap. At speed ratios higher than that in (b), the film thickens as speed ratio increases, while at the same time the wetting line moves through the center of the gap and out into the diverging upstream region. At high speed ratios (c) the metered film would originate upstream of the gap but be

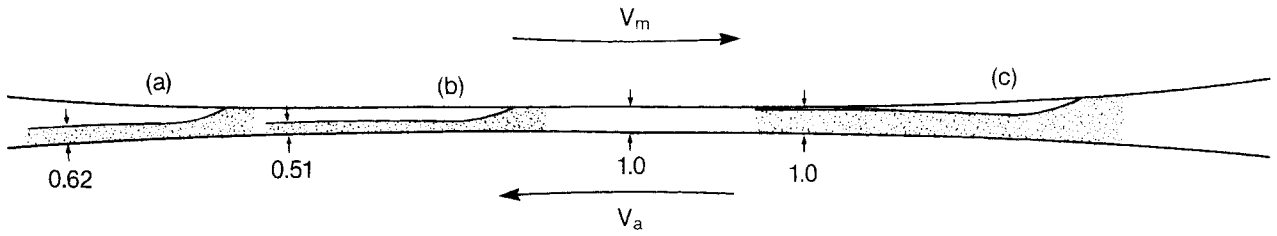

Figure 19. Computed steady-state free surface profiles (Ca = 1.25, Re = 0, St = 0, R/H_o = 1,000, θ_e = 140°).

Speed ratios chosen: a. V_m/V_o = 0; b. V_m/V_a = 0.26, near minimum film thickness; and c. V_m/V_a = 0.42, near apparent onset of cascade where film thickness equals minimum gap thickness.

thicker than the gap, which is not possible in steady-state flow. Instead, when the speed ratio is increased beyond a critical value, a time-dependent flow ensues. When the film becomes as thick as the minimum clearance between the rolls, it reattaches to the metering roll at the gap center. A large air pocket is formed on the metering roll and moves out of the gap with the metering roll surface. With the wetting line at the gap center, the film would tend to be much thinner. But this is not a steady-state flow at this high speed ratio, and so the wetting line is pulled through the gap. As it nears its steady-state position, the film again becomes as thick as the gap. It reattaches to the metering roll, and the cycle begins again.

This process explains the observations of oscillations in the film thickness and the coating bead itself, and the entrainment of large air bubbles on the metering roll. In order to get a crude estimate of the bubble size, one can take the cross-sectional area of the air pocket in Figure 19 and estimate its breakup by analogy with the stability of a hollow jet (Chandrasekhar, 1961, p. 539); the prediction is of spherical bubbles of about 5 gap widths in diameter. For a 0.2-mm (8-mil) gap between 20-cm-dia. (8-in.-dia.) rolls, the bubble diameter should be about 1 mm (40 mil), which is roughly what was observed. This mode of air entrainment is completely different from the high-speed mode observed in plunging tape experiments and curtain coating (cf. Burley and Kennedy, 1975; Blake and Ruschak, 1979; Kistler, 1983).

The one feature of cascade which is not immediately apparent from this analysis is its cross-web structure. At a speed ratio near the onset of cascade, there is presumably a very small clearance between the metering roll and the metered film at the gap center. The air boundary layer brought in on the metering roll would have to turn around near the wetting line and flow back out of the gap. This would create a high-speed, high-shear air flow which could generate waves on the liquid film, and these in turn could cause the meniscus to reattach to the metering roll in an irregular manner. A three-dimensional time-dependent solution of the Navier-Stokes system, including the effect of the air flow, would be required to predict precisely the flow state that exists during the cascade instability.

Computational results in Figure 20a indicate that decreasing the capillary number or increasing the Reynolds number delays the onset of cascade. For a given speed ratio, increasing either surface tension or inertial forces causes the wetting line to locate further from the gap center towards the metered film side of the gap. These trends are confirmed by the data in Figure 20b, which show how inertia shifts the value of speed ratio at which the minimum and the steep upturn of film thickness occur.

Finally, the predicted steady states indicate that changing the gap has little effect on the onset of cascade, which is in general agreement with the data in Figures 13–15. These data do show that, for the half-submerged flow, larger gaps shift the onset of cascade to slightly higher speed ratio, whereas for the unsubmerged flow on the pilot coater the effect is reversed. This may be a subtle secondary effect of the film transfer free surface.

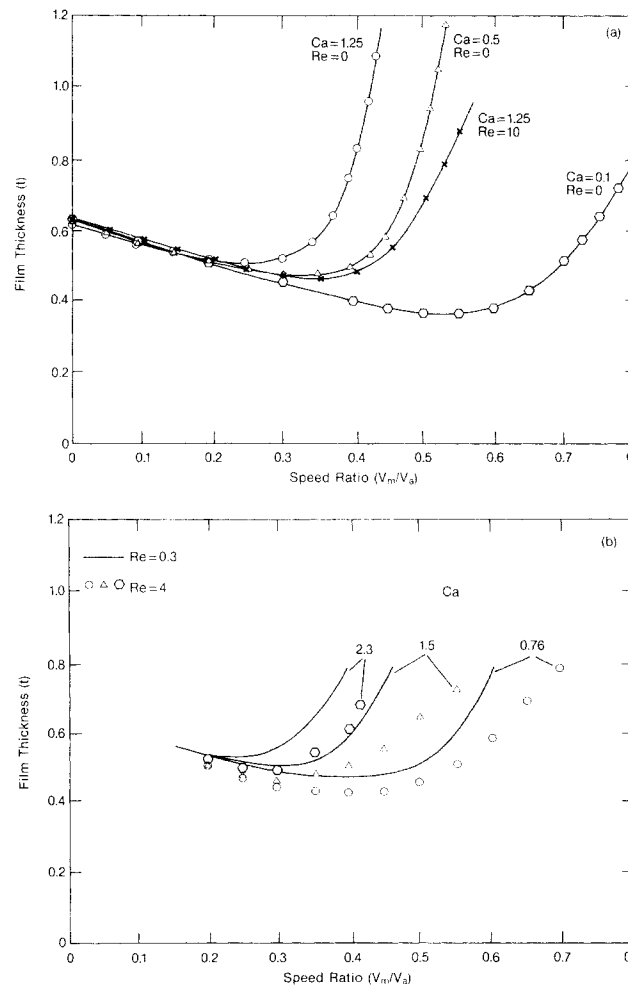

Figure 20. Predicted (a) and measured (b) effect of capillary and Reynolds numbers on the metered film thickness.

Increasing surface tension or inertia lowers the value of the minimum and shifts it to higher speed ratios. The onset of cascade is shifted accordingly.

Conclusions

The flow in the metering gap of a reverse roll coater can be accurately described by two uncoupled half-submerged model flows: film transfer on the upstream feed side of the gap and metered film flow with wetting line on the downstream side. The approximation fails only under extreme circumstances, such as when the film being fed is thinner than the minimum gap between the rolls.

Theoretical analysis and experiments have shown that the key feature of metering gap flow is the flow near the dynamic wetting line and its interaction with the main flow in the gap. It is this region that controls the steady operation and the flow instabilities observed in most reverse roll coaters. Thus, the half-submerged metered film flow model is a good respresentation of flow in a reverse roll coater. The most important phenomena observed in a complete metering gap are predicted by this model. As speed ratio is increased, the dynamic wetting line is drawn into the gap while the coating bead becomes smaller and more tightly curved. As the wetting line passes through the gap, the metered film thickness goes through a minimum and deviates strongly from a lubrication model. The magnitude of the speed ratio at which this happens falls as the capillary number rises. At low speed ratio and low capillary number, there exists a large closed recirculation on the film transfer side of the gap. A small one also may exist near the wetting line. Both could be a source of difficulty in the operation of a coater that applies a liquid that is sensitive to the time spent in the process.

Experimental measurements on various Newtonian liquids have defined the operability of a reverse roll coater. These measurements, combined with computations of steady two-dimensional flows, have led to an understanding of the two major flow instabilities which cause coated film defects in reverse roll coating, namely ribbing and cascade.

In capillary number–speed ratio space, there is a "window" of stable, uniform film flows between the ribbed and cascade flows, although there is evidence that very small amplitude ribs may always be present. This "stable" region expands as gap or Reynolds number is increased. The shape of the stable region becomes more complicated at low capillary number. The stability diagram is not affected by the upstream film-transfer flow as long as the arriving film thickness is larger than the gap. When the arriving film is very thin, the stable region is smaller.

The appearance and disappearance of ribs can be understood in terms of a competition of viscous forces (destabilizing) and surface tension forces (stabilizing) at the metered film free surface. A positive pressure gradient (measured in the flow direction towards the wetting line) tends to make the flow unstable to ribbing. A negative pressure gradient tends to stabilize the flow to ribbing. The latter can be caused by changing either the speed ratio or the capillary number, with the direction of the required change depending on the values of these parameters. The capillary number effect, which can be the opposite of that in forward roll coating, can be traced to the relationship between the wetting line position and the flow domain.

The experiments and theory explain the mechanism of the cascade instability. As speed ratio is increased, the metered film gets thinner (as expected) and the wetting line moves closer to the gap center. At high speed ratios, the wetting line passes through the gap, the metered film gets thicker, and eventually begins to reattach to the metering roll in a cyclic manner. This mechanism has been further confirmed by the flow visualization experiments of DiCarlo (1986).

Thus, the combination of experiments and theory has led to an understanding of the complex flows in a reverse roll coater and the two major flow instabilities to which they are subject. The results clarify the mechanisms governing these phenomena, some aspects of which might at first seem counterintuitive. Further studies are needed of how the flow is influenced by such factors as feed rate and three-dimensional end effects. The effectiveness of doctoring of the metering roll is important and thus needs quantitative evaluation. A quantitative measurement of rib amplitude is needed to resolve the obvious difficulties in measuring the apparent "onset" of the ribbing defect. This could perhaps be done with profilometer traces of a rapidly-solidifed UV-curable coating. Finally, many liquids used in reverse roll coating are non-Newtonian. The Newtonian results demonstrate that the flow involves severe and rapidly changing shear and extensional deformations. Experiments demonstrating the effects of shear-thinning and viscoelastic liquid rheology are examined in a subsequent paper (Coyle et al., 1990a). Predicting and understanding viscoelastic effects remain a considerable challenge.

Acknowledgment

The authors are indebted to the people at James River Graphics, Inc., of South Hadley, Massachusetts, especially Richard D'Amato, Tom Ross, Howard Booth, Mike McGrath, and Bob Lent, both for valuable advice and for the use of their pilot-plant facilities on which much of this work was performed. We are also indebted to the 3M Company for generous financial support, as well as for the advice and insight provided by John Munter, Gary Zvan, Diana Zimny, Don Lewis, and Joe Petrin. We would also like to thank Rick Baune, who assisted in much of the experimental work, and Steve Kistler, who contributed much useful advice. This work was supported by the 3M Company, Westvaco Co., and the University of Minnesota Computer Center.

Notation

B = dimensionless slip coefficient ($\beta\mu/H_o$)
H_o = minimum gap half-width
H_m = thickness of metered film
H_a = thickness of arriving film
f = dimensionless roll separating force ($\int p\,dx/\mu V_a\,[H_o/R]$)
N = wavenumber of ribbing disturbance
P = pressure
p = dimensionless pressure ($PH_o/\mu V_a$)
q = dimensionless flow rate ($\int u\,dy/H_oV_a$)
R = average roll radius $[2/(1/R_a + 1/R_m)]$
R_a = radius of applicator roll
R_m = radius of metering roll
R_c = meniscus radius of curvature
r = dimensionless meniscus radius of curvature (R_c/H_o)
t = dimensionless metered film thickness ($H_m/2H_o$)
u = fluid velocity in flow direction
V_a = applicator roll surface speed
V_m = metering roll surface speed
x = flow direction coordinate
x_w = dimensionless wetting line position ($x/2H_o$)
y = cross-flow direction coordinate
Ca = capillary number (viscous/surface tension force ratio, $\mu V_a/\sigma$)
Re = Reynolds number (inertial/viscous force ratio, $\rho V_aH_o/\mu$)
St = Stokes number (gravity/viscous force ratio, $\rho gH_o^2/\mu V_a$)
σ = surface tension
μ = viscosity

Literature Cited

Babchin, A. J., R. J. Clish, and D. Wahren, "Stability and Disturbance of Coating Films," *Adv. Coll. Int. Sci.*, **14**, 251 (1981).

Benkreira, H., M. F. Edwards, and W. L. Wilkinson, "Roll Coating of Purely Viscous Liquids," *Chem. Eng. Sci.*, **36,** 429 (1981).
Blake, T. D., and K. J. Ruschak, "A Maximum Speed of Wetting," *Nat.* **282,** 489 (1979).
Booth, G. L., *Coating Equipment and Processes,* Lockwood Publishing, New York (1970).
Broughton, G., L. W. Egan, and C. Sturken, "The Reverse Roll Principle of Coating," *TAPPI,* **33,** 314 (1950).
Burley, R., and B. S. Kennedy, "An Experimental Study of Air Entrainment at a Solid/Liquid/Gas Interface," *Chem. Eng. Sci.*, **31,** 901 (1976).
Chandrasekhar, S., *Hydrodynamic and Hydromagnetic Stability,* Oxford University Press, Oxford, England (1961).
Coyle, D. J., "The Fluid Mechanics of Roll Coating: Steady Flows, Stability, and Rheology," PhD Thesis, University of Minnesota, Minneapolis (1984).
Coyle, D. J., C. W. Macosko, and L. E. Scriven, "Film-Splitting Flows in Forward Roll Coating," *J. Fluid Mech.*, **171,** 183 (1986).
———, "Reverse Roll Coating of Non-Newtonian Liquids," *J. Rheol.*, in press (1990a).
———, "Stability of Symmetric Film-Splitting between Counterrotating Cylinders," *J. Fluid Mech.*, in press (1990b).
DiCarlo, M. J., "Reverse Roll Coating—Experiments and Theory," MS Thesis, University of Minnesota, Minneapolis (1986).
Dussan, E. B., "The Moving Contact Line: the Slip Boundary Condition," *J. Fluid Mech.*, **77,** 665 (1976).
Dussan, E. B., and S. H. Davis, "On the Motion of a Fluid-Fluid Interface along a Solid Surface," *J. Fluid Mech.*, **65,** 71 (1974).
Greener, J., and S. Middleman, "Reverse Roll Coating of Viscous and Viscoelastic Liquids," *I and EC Fund.*, **20,** (1981).
Higgins, D. G., "Coating Methods—Survey," *Encyclopedia of Polymer Science Technology,* **3,** 765 (1965).
Ho, W. S., and F. M. Holland, "Between-Roll Metering Coating Technique, a Theoretical and Experimental Study," *TAPPI,* **61,** 53 (1978).
Hocking, L. M., "A Moving Fluid Interface on a Rough Surface," *J. Fluid Mech.*, **76,** 801 (1976).
———, "A Moving Fluid Interface: 2. The Removal of the Force Singularity by a Slip Flow," *J. Fluid Mech.*, **79,** 209 (1977).
Huh, C., and L. E. Scriven, "Hydrodynamic Model of Steady Movement of a Solid/Liquid/Fluid Contact Line," *J. Coll. Interf. Sci.*, **35,** 85 (1971).
Kistler, S. F., "The Fluid Mechanics of Curtain Coating and Related Viscous Free Surface Flows," PhD Thesis, University of Minnesota, Minneapolis (1983).
Kistler, S. F., and L. E. Scriven, "Coating Flows," *Computational Analysis of Polymer Processing,* J. R. A. Pearson and S. M. Richardson, eds., Applied Science Publishers, London and New York, 243 (1983).
Miyamoto, K., "On the Nature of Entrained Air Bubbles in Coating," Paper 86c, AIChE Meeting, New Orleans (Apr., 1986).
Miyamoto, K., and L. E. Scriven, "Breakdown of Air Film Entrained by Liquid Coated on Web," Paper 101g, AIChE Meeting, Los Angeles (Nov., 1982).
Mues, W., J. Hens, and L. Boiy, "Observation of a Dynamic Wetting Process Using Laser-Doppler Velocimetry," *AIChE J.*, **35,** 1521 (1989).
Munch, C., U.S. Pat. 1,847,065 (1932).
Navier, C. L. M. H., "Memoire sur les Lois du Mouvement des Fluides," *Mem. Acad. R. Sci. Inst. Fr.*, **6,** 389 (1827).
Pearson, J. R. A., "The Instability of Uniform Viscous Flow under Rollers and Spreaders," *J. Fluid Mech.*, **7,** (1960).
Pitts, E., and J. Greiller, "The Flow of Thin Liquid Films between Rollers," *J. Fluid Mech.*, **11,** 33 (1961).
Rose, R. C., "The Wiping Roll Coater," *Papier,* **29** (4), 155 (1975).
Savage, M. D., "Cavitation in Lubrication: 2. Analysis of Wavy Interfaces," *J. Fluid Mech.*, **80,** 743 (1977).

Manuscript received Dec. 29, 1988, and revision received Nov. 8, 1989.